condensed matter

MDPI

Review

Readout Methods to Enhance the Performance of Luminescence Thermometers

Miroslav D. Dramićanin [1,*], Abdullah N. Alodhayb [2] and Aleksandar Ćirić [1]

[1] Centre of Excellence for Photoconversion, Vinča Institute of Nuclear Sciences—National Institute of the Republic of Serbia, University of Belgrade, 11351 Belgrade, Serbia; aleksandar.ciric@ff.bg.ac.rs
[2] Department of Physics and Astronomy, College of Science, King Saud University, Riyadh 11451, Saudi Arabia; aalodhayb@ksu.edu.sa
* Correspondence: dramican@vinca.rs

Abstract: Over the past three decades, luminescence thermometry has gained significant attention among researchers and practitioners. The method has progressed in terms of utilizing temperature-sensitive luminescent materials, obtaining temperature read-outs from luminescence, developing applications, and improving performance. This paper reviews and critically analyzes routes for improving luminescence thermometry performance, in particular the sensitivity, accuracy, and precision of the method. These include the use of highly temperature-sensitive probes, temperature read-outs from luminescence with improved sensitivity, multiparameter temperature-reading methods, the applications of principal component analysis and artificial neural networks, and sensor fusion.

Keywords: luminescence thermometry; phosphor thermometry; luminescence; artificial neural networks; sensor fusion

Citation: Dramićanin, M.D.; Alodhayb, A.N.; Ćirić, A. Readout Methods to Enhance the Performance of Luminescence Thermometers. *Condens. Matter* **2024**, *9*, 46. https://doi.org/10.3390/condmat9040046

Academic Editor: Tullio Scopigno

Received: 15 September 2024
Revised: 20 October 2024
Accepted: 5 November 2024
Published: 9 November 2024

1. Introduction

Luminescence thermometry has evolved into a convenient optical method for remote temperature measurements from cryogenic temperatures to 2000 K. Nowadays, it is widely used in a variety of fields. In some of them, such as nanotechnology, biomedicine, and optoelectronics, luminescence thermometry overcomes the limitations of traditional thermometers and provides for better spatial resolution of measurements and thermal imaging. When employing luminescent nanoparticles, this method even allows for local temperature measurements at the nanoscale. Luminescence thermometry exploits temperature-induced changes in the spectral positions of emission and excitation bands, emission band intensities, the shape of emission bands, excited state lifetimes, and emission rise times to determine the temperature of luminescence probes attached to objects of interest. The ample choice of luminescent materials and luminescence features makes luminescence thermometry easily adoptable for a significant number of applications. Many review articles on luminescence thermometry have been published over the years, with recent ones given in refs. [1–15]. However, above all, these articles primarily focus on reviewing and discussing advancements in the development of materials for luminescence thermometry probes, temperature read-outs from luminescence, and the various applications of luminescence thermometry, rarely delving into a comprehensive discussion of measurement performance.

Here, we review and critically analyze methods for enhancing luminescence thermometry performance, keeping in mind that the method's successful use in the future depends on improvements in measurement accuracy and precision. We discuss the approach for the enhancement of measurement sensitivity utilizing luminescence probes that have a strong dependence of their luminescence features on temperature changes. Then, we focus on temperature read-outs from luminescence with the highest measurement sensitivities, such as the multilevel cascade ratiometric method, the single band ratiometric method, and the luminescence intensity squared method. Lastly, we examine and evaluate sophisticated

statistical techniques and machine-learning algorithms that can enhance the precision and accuracy of luminescent thermometry. These include multiparameter linear regression, principal component analysis, artificial neural networks, and sensor fusion.

2. Sensitivity, Accuracy, and Precision of Luminescence Thermometry

It is a common practice in the literature to present calculated absolute and relative sensitivity of luminescence thermometry methods. The main goal is to enable a comparison of thermometry performances when using luminescence probes made from diverse materials. In luminescence thermometry, temperature (measurand, X) is not directly determined. Instead, some indications (Δ), for example, excited state lifetime, emission intensity, and emission intensity ratio are measured and then converted to the temperature value. The absolute (S_a) and relative (S_R) sensitivities of luminescence thermometry are strictly related to the properties of the material that makes the probe; more precisely, they are only related to the extent to which their luminescence properties change with temperature and not to the characteristics of the measurement instrumentation and conditions. They are, respectively, defined as the absolute or relative rate of change in indicator value with the change in measurand value

$$S_a = \left|\frac{d\Delta}{dX}\right| \text{ and } S_R = \left|\frac{1}{\Delta} \times \frac{d\Delta}{dX}\right| \quad (1)$$

However, the absolute and relative sensitivity values are far from sufficient to describe the performance of the luminescence thermometry. The characteristics of measurement instrumentation and measurement conditions significantly influence measurements [16]. Furthermore, for some novel methods of temperature readings from luminescence, such as multiparametric readings and artificial neural networks, it is not possible to reliably derive sensitivity values. Because of this, it would be better to discuss the performance of luminescence thermometry using standard metrology terms like uncertainty in measurement, accuracy, precision, and resolution. From repeated measurement, the estimated value of the measurand ($\overline{X}$) differs from the true value (X_t) [17], see Figure 1. The absolute difference in these values represents the accuracy of the measurement. The true value of the quantity being measured, X_t, lies in the interval $X \pm \delta X$, where X represents value of the measurement and δX its corresponding measurement error. In its simplest consideration, measurement error is a sum of random and systematic (bias) errors: $\delta X = \delta_r X + \delta_b X$ (where r stands for "random" and b for "bias") [18]. In any measurement, random errors are inevitable and arise from variations in experimental settings, noise, and fluctuations in the quantity being measured. The uncertainty in measurement is the standard deviation (σ) of repeated measurements. Precision refers to uncertainty in measurement since it is defined as the inverse of the measurement variance ($p = 1/\sigma^2$). It is important to distinguish between temperature resolution and uncertainty. Temperature resolution is the smallest detectable change in temperature, while standard deviation measures repeatability. For reliable measurements, it is common to set the resolution at twice the standard deviation (2σ), which corresponds to a 95% confidence level. Conventionally, we express the precision limits in terms of a noise floor, which is the noise level below that which one cannot detect signals under the same measurement conditions. Luminescence thermometry frequently calculates it as a product of the measurement standard deviation and the square root of the measurement integration time, expressing it in $K/Hz^{1/2}$.

Other precision limits may be important, depending on the application and material used for the luminescence probe. For instance, when working with nanoparticles, it is crucial to consider the intrinsic thermal fluctuations that can be expressed as

$$\sigma_{th} = T \cdot \sqrt{\frac{k_B}{V \cdot c_v}}, \quad (2)$$

where V is the nanoparticle's volume, c_v is the nanoparticle's constant volume heat capacity, and k_B is the Boltzmann constant. These fluctuations limit the measurement precision to

$1/\sigma_{th}^2$, i.e., it is not possible to improve measurement precision beyond this value. For smaller particles and higher temperatures, σ_{th} becomes larger and the precision limit becomes smaller.

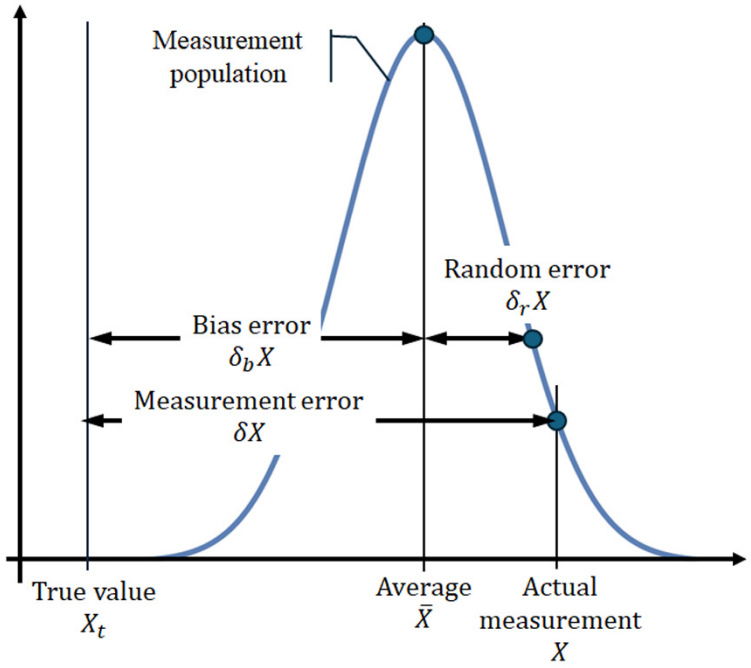

Figure 1. Relationship between measurements and the true value of a measurand. Adapted from Ref. [17].

3. Materials for Luminescence Thermometry Probes with High Sensitivity to Temperature Changes

There is a wide range of luminescent materials available for luminescence thermometry probes. The most popular options are inorganic materials containing activator ions, semiconductor quantum dots, organic dyes, metal–organic frameworks, luminescent polymers, carbon dots, and nanodiamonds [1]. They can take practically any shape or form, including bulk solids and nanoparticles [9]. The thermometric abilities of methods utilizing these materials are highly reliant on the temperature sensitivity of particular luminescent characteristics. Enhanced sensitivity may be achieved using two or more emissions of different origins. This can be realized by using (i) materials doped with two trivalent lanthanide ions (Ln^{3+}) [19–21], (ii) materials doped with one Ln^{3+} and transition metal ion (TM) [22–29], (iii) materials containing both divalent lanthanide ions (Ln^{2+}) and Ln^{3+} [30,31], (iv) semiconductors doped with TM [32,33], and (v) by using defect emissions from host material and Ln^{3+} dopant [34–38]. For example, the ratio of emission intensities from the traps and Sm^{3+} ions in the TiO_2 nanoparticles exhibits sensitivity to temperature fluctuations as high as 10.54%·K^{-1} [35].

However, the sensitivity enhancement in all mentioned approaches comes with some drawbacks. The brightness of double-doped materials may be lower than that of single-doped ones, resulting in a higher measurement uncertainty of emission intensities. Defect emissions are generally of low intensities, again resulting in increased measurement uncertainties. It is difficult to maintain exactly the same concentration of dopants and defects in materials used for probes, which compromises the reproducibility of the measurement methods. Transition metal dopants tend to migrate out of semiconductor nanoparticles, making them useless after a certain time.

4. Temperature Read-Outs from Luminescence with Improved Sensitivity

Luminescence thermometry commonly employs spectral-shape-based techniques specifically measuring the luminescence intensity ratio (LIR) between two emission bands

(ratiometric temperature readout) [1]. This method is important because it is self-referencing, which means that hindrances caused by changes in measurement conditions are avoided by relying on measurements of the ratios of absolute emissions' intensities. Luminescence thermometry probes used with the LIR method typically employ lanthanide-ion- [8] and transition-metal-ion-activated phosphors [2]. These probes utilize the ratio of emission intensities from two adjacent and thermally coupled excited states as a temperature indicator (see Figure 2a).

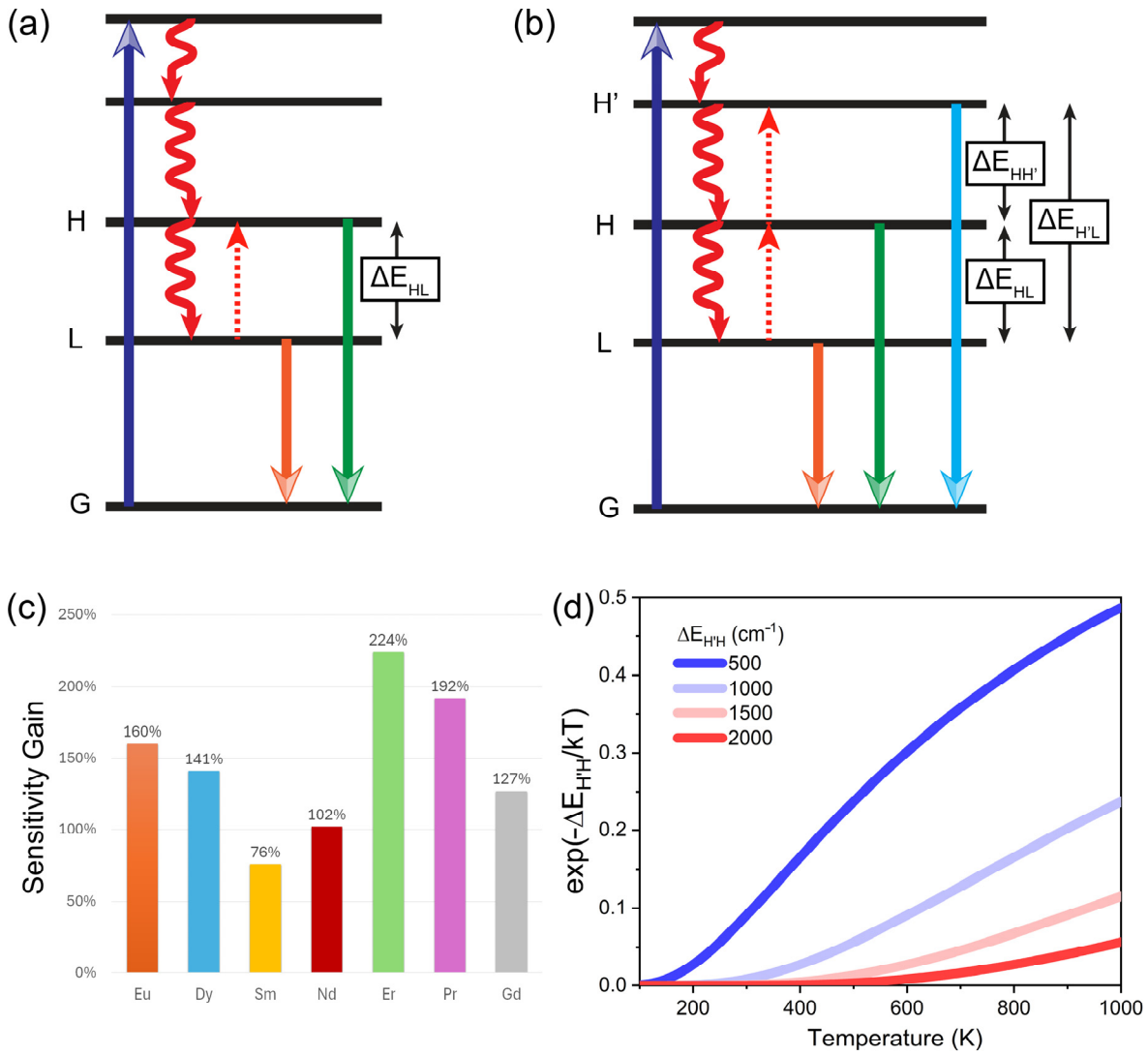

Figure 2. Illustration of the energy levels and emissions associated with (**a**) conventional LIR thermometry and (**b**) multilevel cascade LIR thermometry; (**c**) typical gains in the relative sensitivity of multilevel cascade LIR over conventional LIR for various trivalent lanthanide ions; (**d**) temperature dependences of the normalized ratio of emissions from H′ and H states for varying energy differences between these states, $\Delta E_{H'H}$.

In such instances, the method is generally referred to as Boltzmann-type Luminescence Intensity Ratio (LIR) or Boltzmann thermometry because thermally coupled excited states are populated by the Boltzmann distribution. It is necessary, however, that a thermal equilibrium exists between emitting states which occurs when the thermal exchange rate between the two emissive states is much faster than any competing radiative or nonradia-

tive depopulation rate [39–41]. The ratio of emission intensities from these states may be expressed using a straightforward equation [42]:

$$LIR(T) = \frac{I_H}{I_L} = B \times \exp\left(-\frac{\Delta E_{HL}}{kT}\right). \quad (3)$$

The intensity of the emission from the higher-energy excited state is denoted as I_H, while the intensity of the emission from the lower-energy excited state is denoted as I_L. The energy difference between the thermalized excited states is represented by ΔE_{HL}, and the Boltzmann constant is denoted as k (k = 0.695 cm^{-1}·K^{-1}). Further, $B = \nu_H A_H g_H / \nu_L A_L g_L$, where A is the radiative transition probability, ν is the emission barycenter frequency, and g is the level degeneracy. In this method, the relative sensitivity of LIR decreases constantly as temperature increases. The relative sensitivity is determined only by the energy difference between the excited states that provided emissions for LIR. A larger energy difference corresponds to a higher relative sensitivity:

$$S_R\left[\%K^{-1}\right] = \left|\frac{1}{LIR} \times \frac{dLIR}{dT}\right| \cdot 100\% = \frac{\Delta E_{HL}}{kT^2} \cdot 100\%. \quad (4)$$

In terms of relative sensitivity, this method has a limitation when used with trivalent lanthanide ions since the sensitivity is proportional to the energy difference between thermally coupled states, and the largest energy difference of about 1750 cm^{-1} is in the Eu^{3+} ($^5D_1$ and $^5D_0$ excited levels). This provides for 2.8% K^{-1} relative sensitivity at 300 K. Table 1 lists typical values of relative sensitivities at 300 K for other trivalent lanthanide ions, excited levels that provide emissions for LIR, and the typical energy difference between these levels. Furthermore, the value of relative sensitivity rapidly decreases with an increase in temperature, negatively affecting the measurement precision at high temperatures. Transition-metal-activated phosphors can also facilitate the realization of the LIR method. In cases of Mn^{4+} and Cr^{3+}, the LIR is derived from the emission intensity ratio of the $^4T_2 \rightarrow {}^4A_2$ and $^2E \rightarrow {}^4A_2$ transitions (relative sensitivity at 300 K in the 1.2–2.6% K^{-1} range) [43–46], while in cases of Mn^{5+}, emissions from ^1E and $^3T_2$ are exploited (relative sensitivity at 300 K around 2.0% K^{-1}) [47,48].

Table 1. Typical room temperature relative sensitivities of LIR thermometers that utilize trivalent lanthanide ions involve excited states and energy gaps between them, a third excited state used in the multilevel cascade LIR, and a sensitivity gain of the multilevel cascade LIR over the conventional LIR.

Ion	Eu^{3+}	Dy^{3+}	Sm^{3+}	Nd^{3+}	Er^{3+}	Pr^{3+}	Gd^{3+}
Excited levels	$^5D_1$, $^5D_0$	$^4I_{15/2}$, $^4F_{9/2}$	$^4F_{3/2}$, $^4G_{5/2}$	$^4F_{5/2}$, $^4F_{3/2}$	$^2H_{11/2}$, $^4S_{3/2}$	$^3P_1$ + $^1I_6$, $^3P_0$	$^6P_{5/2}$, $^6P_{7/2}$
Emission color	Green/Orange	blue	Green/Orange	NIR	Green	Blue	UV
ΔE_{HL} [cm^{-1}]	1750	900	1250	1000	780	600	500
Relative sensitivity [%K^{-1}]	2.80	1.44	2.00	1.60	1.25	0.96	0.80
Third excited level	$^5D_2$	$^4G_{11/2}$	$^4G_{7/2}$	$^4F_{7/2}$	$^4F_{7/2}$	$^3P_2$	$^6P_{3/2}$
Sensitivity gain [%]	160	141	76	102	224	192	127

4.1. Multilevel Cascade LIR Method

A way to increase the LIR method's sensitivity is to use emissions from excited states that have a large energy difference between them (see Figure 2b). Tian et al. [49] have shown that when there is a thermal equilibrium between the first (L) and second excited state (H) and between the second (H) and third excited state (H′), the populations of the first and third excited states will follow Boltzmann's distribution in a cascade thermalization scheme with a larger energy difference of $\Delta E_{H'L} > \Delta E_{HL}$. This method has been effectively validated using Boltzmann thermometers utilizing Dy^{3+} [50,51], Er^{3+} [52], and Gd^{3+} [53], demonstrating its enhanced levels of relative sensitivity in each instance. The method can be applied to a wide range of trivalent lanthanide ions with a typical gain in relative

sensitivity displayed in Figure 2c. The sensitivity gain is given by the ratio of sensitivities when using the H′ level and H level.

However, the method's improved sensitivity over conventional LIR does not necessarily result in better measurement precision. Emissions from the third excited state ($I_{H'}$) generally have a lower intensity than those from the second excited level:

$$\frac{I_{H'}}{I_H} = \frac{\nu_{H'} A_{H'} g_{H'}}{\nu_H A_H g_H} \times \exp\left(-\frac{\Delta E_{H'L} - \Delta E_{HL}}{kT}\right) = \frac{\nu_{H'} A_{H'} g_{H'}}{\nu_H A_H g_H} \times \exp\left(-\frac{\Delta E_{H'H}}{kT}\right). \quad (5)$$

This is because high-energy excited states require high temperatures to gain population. The higher energy difference to the second excited state ($\Delta E_{H'H}$), the higher temperature is needed to facilitate emission (see Figure 2d). This induces two significant consequences. First, the method only works at temperatures sufficient enough to facilitate emissions and, therefore, has a smaller operational range than the conventional LIR. Secondly, the measurement uncertainty of emission intensity from a high-energy excited level is greater than that of the second excited level. Consequently, the improvement in temperature measurement precision may not occur despite the larger measurement sensitivity. Based on the literature data and our analysis, we can conclude that this method may only improve luminescence thermometry performance at high temperatures.

Ćirić et al. [54] extended this approach by introducing the multi-cascade LIR, Figure 3a, that exploits emissions from several Dy^{3+} high-energy excited states. The use of emission from excited energy states located at approximately 5000 cm^{-1} above the first excited state allowed for a fivefold larger relative sensitivity than in the conventional LIR (see Figure 3b). However, the method's applicability was limited to temperatures greater than 650 K. The further application of this method saw a significant improvement in the relative sensitivity of luminescence thermometers based on Er^{3+} upconversion emissions [52], while combining this method with multiparametric linear regression led to a thirty-fold increase in the relative sensitivity of Dy^{3+} thermometers [55].

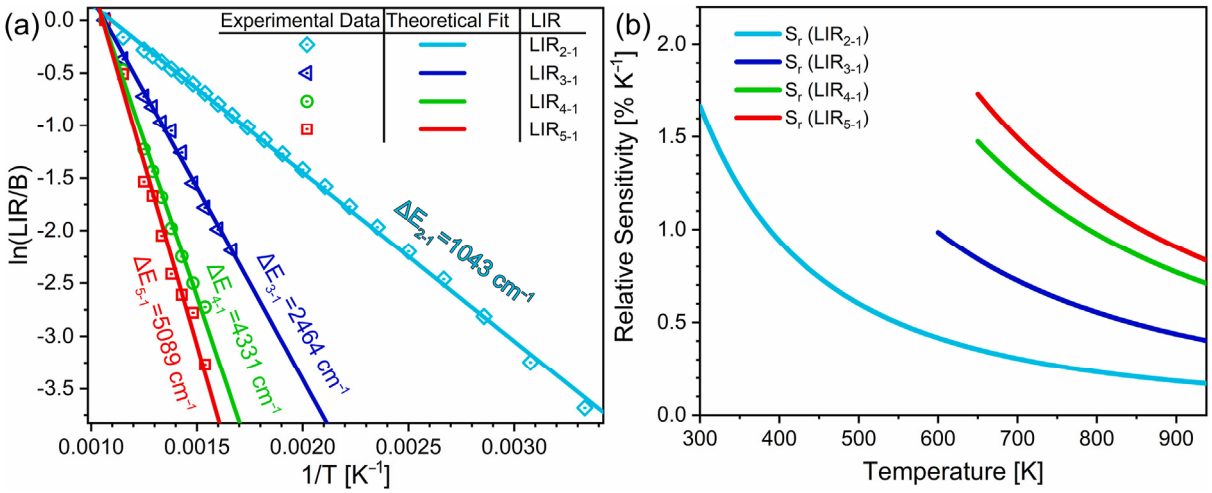

Figure 3. (**a**) LIR dependence on inverse temperatures. $LIR_{2\text{-}1}$ is a conventional LIR while $LIR_{3\text{-}1}$, $LIR_{4\text{-}1}$, and $LIR_{5\text{-}1}$ exploit emissions from high-energy excited states. (**b**) corresponding relative sensitivities. Reproduced from ref. [54] with permission.

4.2. Dual-Excited Single Band Ratiometric (SBR) Method

A dual-excited single-band ratiometric thermometry (SBR) method [56] compares the strengths of two emissions from the same state after being excited from the ground state (G) and the first excited state (G′); see Figure 4a. In other words, the temperature readout is performed by first exciting from the ground level and observing a dominant emission, and then exciting from the excited level thermalized with the ground level and observing the same emission as in the first step. As in other types of LIR techniques, a

thermal equilibrium must exist between G and G′ states, which are separated by the energy difference of $\Delta E_{GG'}$. Then, the expressions describing this intensity ratio, LIR_{SBR}, and its relative sensitivity have the same forms as for the conventional and multicascade LIRs:

$$LIR_{SBR}(T) = \frac{I_{G'}}{I_G} = B_{GG'} \times \exp\left(-\frac{\Delta E_{GG'}}{kT}\right), \quad (6)$$

$$S_{R-SBR}\left[\%K^{-1}\right] = \frac{\Delta E_{GG'}}{kT^2} \cdot 100\%. \quad (7)$$

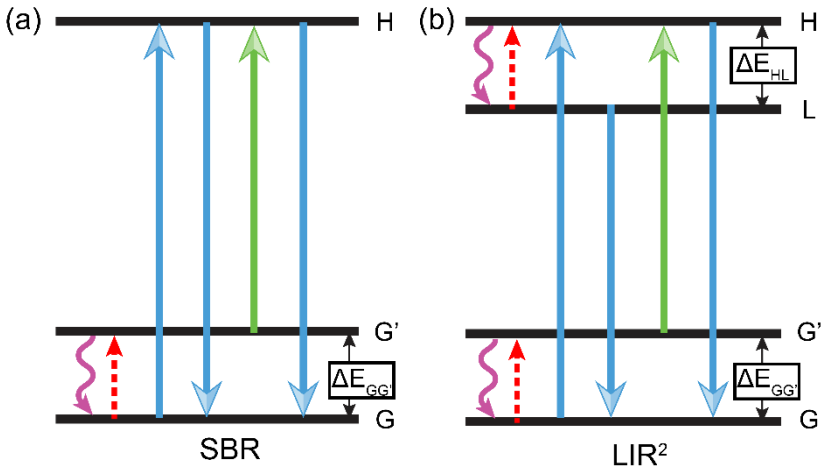

Figure 4. Illustration of the energy states, excitations, and emissions involved in (**a**) single band ratiometric (SBR) thermometry and (**b**) luminescence intensity squared thermometry (LIR^2).

Relative sensitivity values of the method linearly depend on the energy difference between states from which excitation occurs, $\Delta E_{GG'}$. This energy gap can be substantially larger than energy gaps in the conventional LIR, providing for better relative sensitivity with similar uncertainty in emission intensity determination. For example, at the temperature of 300 K, the SBR method has 3.57%K^{-1} relative sensitivity when using excitations from $^6H_{9/2}$ and $^6H_{5/2}$ Sm^{3+} states having a 2230 cm^{-1} energy difference between them. With Pr^{3+} $^3H_5$ and $^3H_4$ states (energy difference $\simeq$ 2160 cm^{-1}), Tb^{3+} $^7F_5$ and $^7F_6$ states (energy difference $\simeq$ 2060 cm^{-1}), and Nd^{3+} $^4I_{11/2}$ and $^4I_{9/2}$ states (energy difference $\simeq$1860 cm^{-1}), SBRs relative sensitivities at 300 K are 3.48%K^{-1}, 3.29%K^{-1}, and 2.97%K^{-1}, respectively. These are much larger values when compared with those for the conventional LIR given in Table 1. Further combinations of energy states that are appropriate for SBR can be achieved with these or other trivalent lanthanide ions due to their abundance of energy levels [57,58].

In addition to enhanced sensitivity, the SBR technique offers two additional advantages compared with the conventional LIR. The $B_{GG'}$ and $\Delta E_{GG'}$ can be extracted directly from the photoluminescence emission spectrum without the need for any fitting. $B_{GG'}$ is determined by dividing the total emissions for transitions that end at the G and G states, while $\Delta E_{GG'}$ is determined by subtracting the energies of the barycenters of these emissions [56]. Furthermore, out of all the available ways for measuring temperature using luminescence thermometry, the SBR method requires the simplest sensor setup [59]. The main disadvantages of the SBR include the requirement for measurement correction owing to temperature-induced changes in bandwidth, as demonstrated by Zhou et al. [60], and the need for constant excitation change during the measurement.

4.3. Luminescence Intensity Squared Method

The luminescence intensity ratio squared (LIR^2) approach, as shown in Figure 4b, combines the traditional luminescence intensity ratio (LIR) method with the dual-excitation single-emission band ratiometric (SBR) approach. In the first step, the ion is excited from the ground state G and the emission from the L level is observed. In the second step the

excitation is performed from the G′ level, and the emission from the H level is observed. The ratio of those two emissions gives LIR^2. It leverages by using two thermalizations, which in turn provide for a high sensitivity, equal to the sum of the conventional LIR and SBR sensitivities [61]:

$$S_{R-LIR^2} = S_R \times S_{R-SBR}, \quad (8)$$

since

$$\Delta E_{LIR^2} = \Delta E_{HL} + \Delta E_{GG'} \text{ and } LIR^2 = LIR \times LIR_{SBR} \quad (9)$$

As mentioned earlier in the text, a large energy difference between thermalized states is required to achieve high sensitivity. In this case, two pairs of energy states with a smaller energy difference than the total energy contributing to the sensitivity value should fulfill the thermalization conditions. The method maintains uncertainty in the emission intensity determination of both methods. With a higher sensitivity and the same uncertainty, the LIR^2 should have better precision than the LIR and SBR.

One can also construct the LIR^2 with two ions by applying SBR to one and LIR to the other. The typical example is given by Ćirić et al. [62] using $Y_3Al_5O_{12}$: Er^{3+}/Yb^{3+} emission. The SBR excitation scheme was applied to Yb^{3+} (on Stark components of Yb^{3+} $^2F_{7/2}$ ground state) while the LIR scheme was utilized with Er^{3+} excited states. Researchers looked at LIR, SBR, and LIR^2 methods on the same material and found that LIR^2 is better than LIR and SBR in terms of sensitivity, temperature resolution, and measurement range in both visible (see Figure 5a) and near-infrared (see Figure 5b) spectral regions.

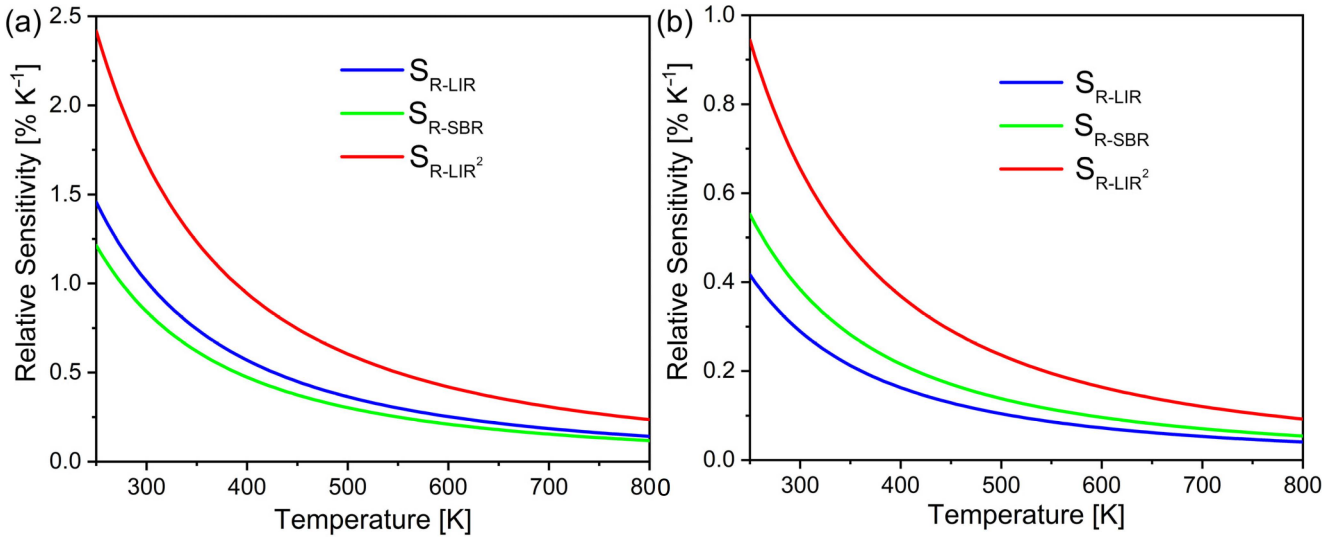

Figure 5. Relative sensitivities of LIR, SBR, and LIR^2 methods based on $Y_3Al_5O_{12}$:Er^{3+}/Yb^{3+} emissions in (**a**) visible and (**b**) near-infrared spectral regions. From ref. [62] with permission.

4.4. Time-Resolved Single-Band Ratiometric Luminescence Thermometry

The time-resolved single-band ratiometric luminescence thermometry (TSBR) takes the ratio of emission intensities measured at the different time delays after excitation. It requires a probe that consists of two materials that emit over the same spectral region but have drastically different emission decay times. Qiu et al. [63] introduced the method using nanomaterials, which included 3.5 nm large PbS quantum dots and 12 nm large $NaYbF_4$:0.5%Tm@$NaYF_4$:10%Yb@$NaYF_4$:50%Nd nanophosphors. In their study, quantum dots were emitted at 814 nm with a very short decay time, while nanophosphor was emitted at 804 nm with a long lifetime. The method provided a relative sensitivity of up to 5.6% K^{-1} and a precision of 0.5 K at 45 °C. In contrast to other spectral-shape-based techniques, this method requires emission measurements at only one spectral region.

5. Advanced Data Processing for Improved Precision and Accuracy of Luminescence Thermometry

Luminescence thermometry typically utilizes a small portion of the luminescence data to measure temperature. This is because traditional temperature measurements are based entirely on temperature-induced variations in the characteristics of specific emission lines or their emission kinetics. The latest techniques to enhance the precision and accuracy of luminescence thermometry involve simultaneously utilizing multiple luminescence properties of materials. These approaches presuppose that concurrently observing numerous parameters will better accumulate temperature-induced alterations in luminescence characteristics, augmenting measurement sensitivity. If there are no artifacts present in the data, then all the thermal readings should converge. Nevertheless, incorporating additional spectral features increases the uncertainty in temperature estimation and may cancel the advantages.

We can divide the strategies in question into three categories. All of them use multiple temperature indicators based on different spectral features or even complete emission spectra. The first group includes multimodal [64–68] and multiparameter methods [69–73]. In multimodal methods, different temperature indicators based on different luminescence features of the same material are not used for temperature measurements at the same time. Instead, each one is seen as a sensor for a different temperature region or as a concurrent sensor. Multiparameter methods, on the other hand, combine individual temperature indicators into a single indicator, typically using linear multiparameter regression. In the second group are methods for reducing the amount of data, like principal component analysis (PCA) and t-distributed stochastic neighbor embedding (t-SNE) [74–76]. The third group includes approaches that utilize artificial neural networks [77,78]. An additional approach includes the use of a support vector machine [79].

5.1. Multiparameter Methods Based on Multiple Linear Regression

Multiple linear regression (MLR) is a statistical technique that uses multiple explanatory variables to predict the outcome of a response variable. Every value of the independent variable is linked to a value of the dependent variable. The linear relationship between the thermometric parameters Δ (independent variables) and temperature (dependent variable) can be represented using the equation of multiple linear regression:

$$T = \beta_0 + \sum_{i=1}^{n} \beta_i \cdot \Delta_i + \varepsilon, \tag{10}$$

where β_0 is the constant term (T-intercept), $\beta_1, \ldots, \beta_n$ are the slope coefficients for each of n explanatory variables, and ε is the model's error term (also known as the residuals).

To utilize MLR, it is necessary to have a linear relation between the dependent and independent variables, with each of them being continuous functions. Additionally, the independent variables must not be correlated with one another. While not strictly necessary, it is beneficial for the values of independent variables to be within the same range, as fitting algorithms infer that larger values carry greater relevance. For this purpose, one can apply feature scaling. Apart from putting values of independent variables in the same range, feature scaling provides for the easier interpretation of results.

Alrebdi et al. [48] proposed a novel approach to scale and linearize explanatory variables by representing the temperature dependence on temperature indicator variables using equations of state. The authors conducted a comparison of the accuracy and precision of three single-parameter thermometry methods that rely on $Ca_6BaP_4O_{17}$:Mn^{5+} near-infrared emission. The emission spectrum of this phosphor shows a narrow emission band from the $^1E \rightarrow {}^3A_2$ intra-configurational transition around 1140 nm, followed by vibrational sidebands [47]. The thermometry methods involved measuring the luminescence intensity ratios between emissions from the ^1E and $^3T_2$ states—LIR_1, between Stokes and anti-Stokes emission sidebands—LIR_2, and the ^1E energy—E_{1E}. They also evaluated a multiparam-

eter thermometry approach that incorporates all three indicators. The results showed (see Figure 6) that the multiparametric method provides better accuracy and precision than the LIR_2 and E_{1E} single-parameter methods and approximately equal results as the LIR_1 method.

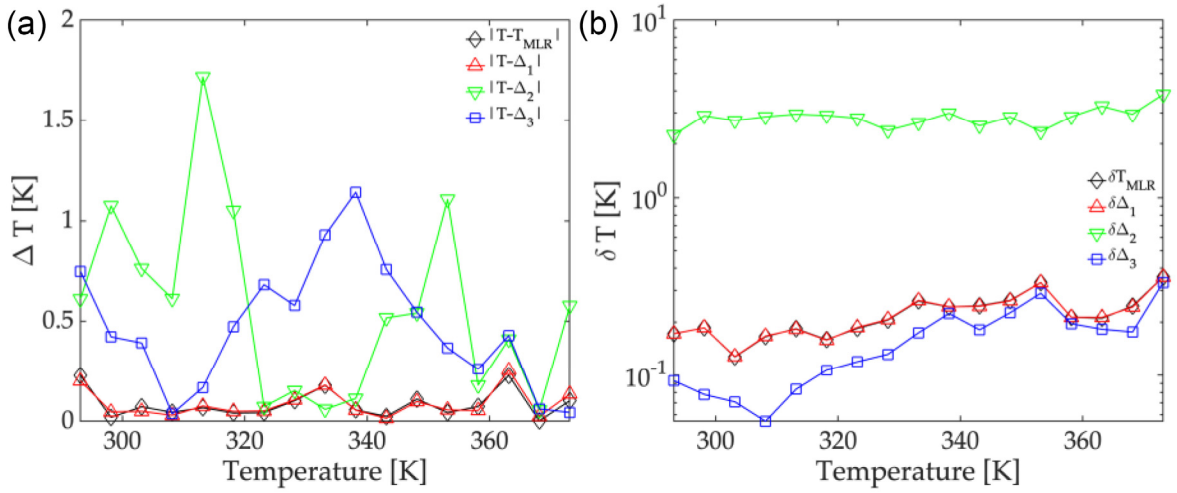

Figure 6. (**a**) The accuracy (ΔT) and (**b**) the precision (δT) of single-parametric (LIR_1—red Δ symbol and line, LIR_2—green ∇ symbol and line, and E_{1E}—blue $\square$ symbol and line) and multiparametric temperature (black $\Diamond$ symbol and line) readings from the near-infrared emission of $Ca_6BaP_4O_{17}$:Mn^{5+} at different temperatures. From ref. [48].

Given that most luminescence temperature indicators are not linearly proportional to temperature, the method requires either the linearization of these relationships or applications over a very narrow temperature range where linear relations can be assumed. Therefore, it can be beneficial to extend the approach using multiple nonlinear regression. However, no one has demonstrated this approach yet.

5.2. Principal Component Analysis for Luminescence Thermometry

Gathering all changes in luminescence spectra caused by temperature variations can produce the maximum sensitivity of luminescence thermometry. However, to make a practical temperature sensor, it is necessary to have one indicator (a few for multiparametric methods) that is a monotonic function of temperature. The application of data reduction methods in luminescence thermometry is based on the idea of reducing the entire emission spectrum from the sample to a single value for temperature determination. Principle component analysis (PCA) is an unsupervised machine-learning technique that transforms the original dataset into parameters known as principal components (PCs). These PCs maintain all the various present in the original dataset, but the first principal component encompasses the largest number of these variances. Therefore, we can use the first principal component as a temperature indicator. Furthermore, PCA provides information about spectral regions where large changes in luminescence occur due to temperature changes. We can further exploit this information to eliminate low-sensitive spectral regions from measurements, thereby reducing measurement time and uncertainty.

Jelić et al. [80] applied PCA to emission spectra of $GdVO_4$:Sm^{3+} measured at different temperatures. They demonstrated that scores on the first three PCs derived from spectra measured at similar temperatures tend to cluster together. However, they did not use PCs as temperature indicators. Šević et al. [75] employed PCA to differentiate the Sr_2CeO_4:Eu^{3+} emission spectrum measured at different temperatures. The authors were able to predict the temperature within a 95% confidence level.

Rajić et al. [76] recently used PCA to reduce the emission spectra of Pr^{3+}-doped YF_3 that were recorded at different temperatures to PCs. They discovered that the first PC accounts for 99.3% of the temperature-induced variance in the emission spectra. Using this

PC as an indicator of temperature, they designed the luminescence thermometry method, which has an average accuracy of 0.7 K and a measurement uncertainty of 0.5 K.

5.3. The Use of Artificial Neural Networks in Luminescence Thermometry

Artificial neural networks (ANNs) are the most widely used supervised machine-learning methods and have significantly transformed data processing [81]. While the application of ANNs in luminescence thermometry is still in its early stages, the growing accessibility of processing power and user-friendly libraries has made it more convenient for researchers to investigate the potential advantages of this technology. Specifically, it is crucial to investigate and harness the capabilities of ANNs to enhance the accuracy and precision in luminescent thermometry.

Liu et al. [82] have described a luminescence thermometry method that uses ANN recognition from rhodamine B emission to determine the sample temperature. The authors used ANNs with two types of data: one based on the integrated emission intensity and emission peak intensity, and the other on a selection of 80 values between 550 nm and 660 nm of normalized spectra, thus representing the spectral shape. The second approach had better measurement accuracy because normalized spectra were not affected by excitation laser light fluctuation, and because this set contained a larger number of temperature-dependent spectral features. Simple feedforward ANNs containing two hidden nodes have been used by Munro et al. [83] to recognize temperature from emissions of CdSe/ZnS quantum dots. The authors tested five sets of input data containing different spectral features and found that the ANN based on the normalized emission intensity provides the greatest accuracy (RMS uncertainty of 0.29 K). Lewis et al. [73] used a dense fully connected neural network to measure the temperature in a microfluidic device filled with CdTe quantum dots. The input was normalized emission spectra and emission decays. The method provided a temperature accuracy of 0.4 K for cryogenic temperatures and 0.1 K around room temperature. Cui et al. [78] employed a one-dimensional Convolutional Neural Network (CNN) structure to develop a method to determine the temperature based on the emission of $Y_3Al_5O_{12}$:Cr^{3+}. A Convolutional Neural Network (CNN) is a type of artificial neural network that has a significantly lower number of network parameters to compute. This characteristic makes the network more manageable to optimize and reduces the likelihood of overfitting [84]. The average measurement error of the method in the range of 35–315 °C was 0.20 °C, much smaller than the 1.31 °C obtained with classical ratiometric thermometry and the 1.69 °C obtained with a multiple linear regression method. Long short-term memory neural networks (LSTM), a type of recurrent neural network [85], can be used for obtaining the high-frequency 2D surface temperature field information from Mg_4FGeO_6:Mn^{4+}-coating luminescence with very high accuracy, as shown by Cai et al. [86].

5.4. Sensor Fusion Luminescence Thermometry

Sensor fusion is the procedure of merging sensor data or data obtained from different sources in a manner that reduces the uncertainty in the resulting information compared with using these sources separately. Ćirić et al. demonstrated that this modern sensor science method has great potential to increase the precision of luminescence thermometry [87]. In luminescence thermometry, the sensor fusion can utilize separate luminescence thermometry sensors or several temperature indicators from one sensor (similar to multiparameter methods). Figure 7a schematically shows the application of this basic sensor fusion method to luminescence thermometry. The "fused" temperature (T_F) from N sensors can be calculated as follows [87]:

$$T_F = \frac{1}{\frac{1}{\sigma_1^2} + \frac{1}{\sigma_2^2} + \cdots + \frac{1}{\sigma_N^2}} \left(\frac{T_1}{\sigma_1^2} + \frac{T_2}{\sigma_2^2} + \cdots + \frac{T_N}{\sigma_N^2} \right), \quad (11)$$

where T_i (i = 1, 2, …, N) are mean temperatures obtained from N temperature sensors and σ_i^2 are their respective variances. The fused result is a linear combination of the N

measurements weighted by their respective noise variances. The variance of the "fused" temperature measurement

$$\sigma_F^2 = \frac{1}{\frac{1}{\sigma_1^2} + \frac{1}{\sigma_2^2} + \cdots + \frac{1}{\sigma_N^2}} \quad (12)$$

is smaller than the variance of individual sensors. For example, in the case of N sensors having the same variance σ^2, the variance of the "fused" measurement will be $\sigma_F^2 = \sigma^2/N$.

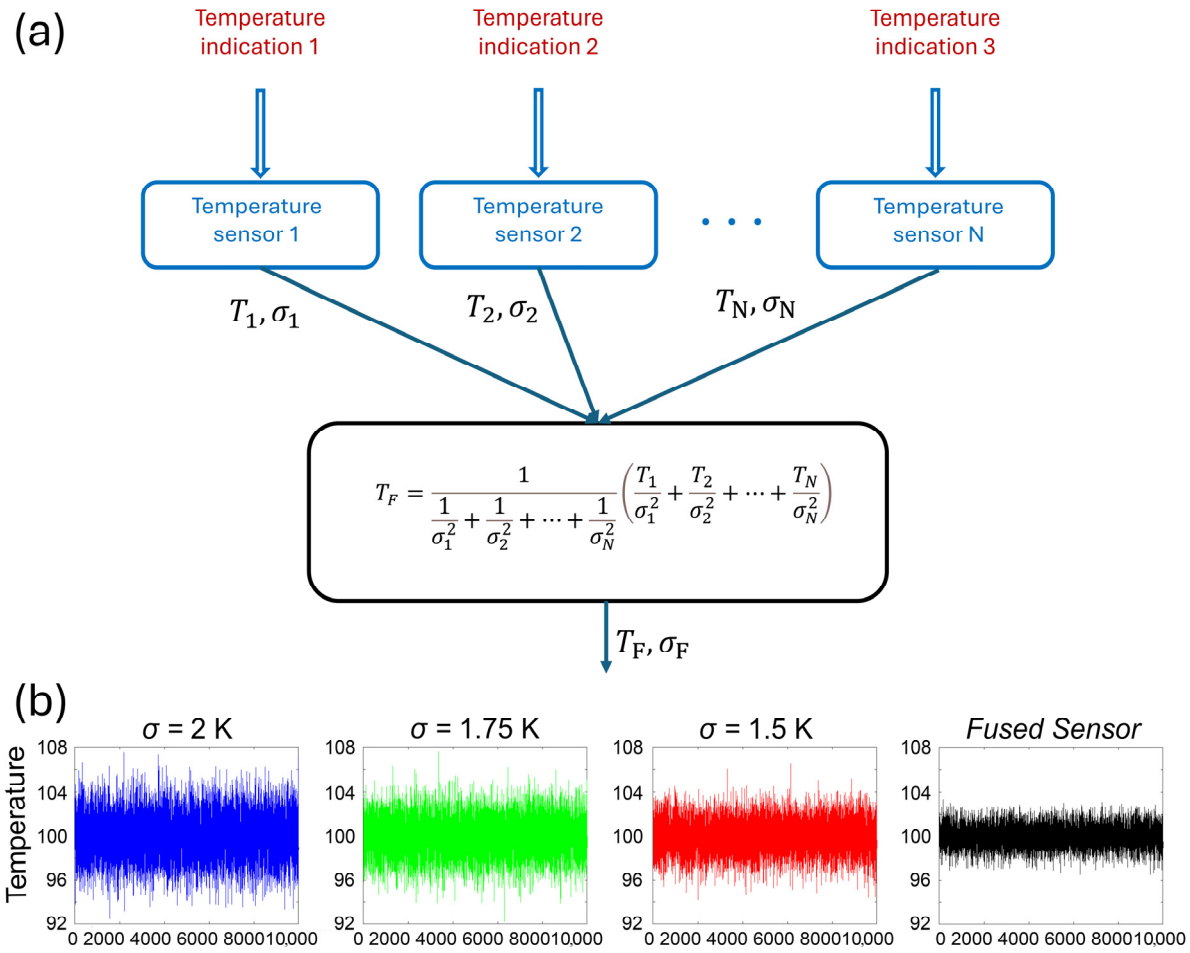

Figure 7. (**a**) Flowchart of a simple sensor fusion luminescence thermometry (SFLT); (**b**) simulation of temperature readings at 100 °C nominal temperature, using sensors with standard deviations of 2 °C (blue line), 1.75 °C (green line), 1.5 °C (red line), and the fused reading from three sensors using Equation (10) (black line) that has a reduced standard deviation of 0.9795 °C.

Figure 7b illustrates a numerical simulation of three temperature readings at a nominal temperature of 100 °C, using sensors with standard deviations of 2 °C (blue line), 1.75 °C (green line), and 1.5 °C (blue line). The figure clearly shows that the fused temperature obtained from these three sensors (black line) has a much smaller standard deviation (σ_F = 0.99 °C).

6. Conclusions

The predominant focus of previous research on enhancing luminescence thermometry performance has been on the advancement of luminescent probes that exhibit exceptional sensitivity to variations in temperature. The reports seldom examined and discussed the potential impact of the increased temperature sensitivity of luminescent temperature indicators on measurement accuracy and precision. In reported cases, the enhancement of sensitivity often led to an increase in measurement uncertainties for luminescence

temperature indicators, thereby reversing the positive effects of increased sensitivity on accuracy and precision. Luminescence probes that rely on two luminescent centers may face challenges in the reproducibility of their preparation process, particularly in maintaining consistent dopant concentrations. This may be a serious problem for probes exhibiting emissions from defects in their structure. Advanced methods based on ratios of emission intensities show better measurement sensitivities compared with the traditional intensity ratio method. Multilevel cascade LIR may be an excellent way to overcome the sensitivity limitation of the conventional LIR at high temperatures, where emissions from high-energy states gain significant intensities. SBR provides slightly higher sensitivity than conventional LIR, with the same uncertainty in determining emission intensity but requires two consecutive emission measurements after excitations with different energies. According to our assessment, LIR^2 has the highest capacity to enhance the accuracy and precision of ratiometric luminescence thermometry. This is because it combines the sensitivities of conventional LIR and SBR, without affecting the thermalization process or introducing additional uncertainty in determining emission intensity. PCA and artificial neural networks are the most promising ways to enhance measurement performance when it comes to determining temperature from luminescence with the help of modern statistical techniques and machine-learning algorithms. The reason for this is that they can effectively harness a significant number of temperature-induced fluctuations in luminescence for temperature determination, which surpasses the capabilities of a system relying on a single luminescent temperature indicator. Finally, sensor fusion in luminescence thermometry has been proven to significantly reduce uncertainty in estimating temperature from multiple independent sensors or indications.

Author Contributions: Conceptualization, M.D.D.; methodology, M.D.D. and A.N.A.; formal analysis, M.D.D., A.Ć. and A.N.A.; writing—original draft preparation, M.D.D. and A.Ć.; writing—review and editing, M.D.D.; visualization, M.D.D. and A.Ć. All authors have read and agreed to the published version of the manuscript.

Funding: This research was supported by the Science Fund of the Republic of Serbia, #GRANT No 7017, TECHNOLOGY FOR REMOTE TEMPERATURE MEASUREMENTS IN MICROFLUIDIC DEVICES—REMTES (M.D. Dramićanin, A. Ćirić). A. N. Alodhayb would like to extend its sincere appreciation to the Researcher supporting program at King Saud University, Riyadh, for funding this work under the project number (RSP2024R328). M.D. Dramićanin and A. Ćirić would like to acknowledge funding of the Ministry of Science, Technological Development, and Innovation of the Republic of Serbia under contract 451-03-66/2024-03/200017.

Data Availability Statement: The data will be available upon request.

Conflicts of Interest: The authors declare no conflict of interest.

References

1. Bednarkiewicz, A.; Drabik, J.; Trejgis, K.; Jaque, D.; Ximendes, E.; Marciniak, L. Luminescence based temperature bio-imaging: Status, challenges, and perspectives. *Appl. Phys. Rev.* **2021**, *8*, 011317. [CrossRef]
2. Marciniak, L.; Kniec, K.; Elżbieciak-Piecka, K.; Trejgis, K.; Stefanska, J.; Dramićanin, M. Luminescence thermometry with transition metal ions. A review. *Coord. Chem. Rev.* **2022**, *469*, 214671. [CrossRef]
3. Brites, C.D.S.; Marin, R.; Suta, M.; Carneiro Neto, A.N.; Ximendes, E.; Jaque, D.; Carlos, L.D. Spotlight on Luminescence Thermometry: Basics, Challenges, and Cutting-Edge Applications. *Adv. Mater.* **2023**, *35*, e2302749. [CrossRef]
4. Brites, C.D.S.; Balabhadra, S.; Carlos, L.D. Lanthanide-Based Thermometers: At the Cutting-Edge of Luminescence Thermometry. *Adv. Opt. Mater.* **2019**, *7*, 1801239. [CrossRef]
5. Quintanilla, M.; Henriksen-Lacey, M.; Renero-Lecuna, C.; Liz-Marzán, L.M. Challenges for optical nanothermometry in biological environments. *Chem. Soc. Rev.* **2022**, *51*, 4223–4242. [CrossRef] [PubMed]
6. Stefańska, J.; Bednarkiewicz, A.; Marciniak, L. Advancements in excited state absorption-based luminescence thermometry. *J. Mater. Chem. C* **2022**, *10*, 5744–5782. [CrossRef]
7. Zhou, J.; del Rosal, B.; Jaque, D.; Uchiyama, S.; Jin, D. Advances and challenges for fluorescence nanothermometry. *Nat. Methods* **2020**, *17*, 967–980. [CrossRef]
8. Kumar, P.; Patel, R.; Shrivastava, N.; Patel, M.; Rondeau-Gagné, S.; Selopal, G.S. Aspects of luminescence nanoprobes for thermometry: Progress and outlook. *Appl. Mater. Today* **2023**, *35*, 101931. [CrossRef]

9. Suta, M. Performance of Boltzmann and crossover single-emitter luminescent thermometers and their recommended operation modes. *Opt. Mater. X* **2022**, *16*, 100195. [CrossRef]
10. Harrington, B.; Ye, Z.; Signor, L.; Pickel, A.D. Luminescence Thermometry Beyond the Biological Realm. *ACS Nanosci. Au* **2024**, *4*, 30–61. [CrossRef]
11. Jahanbazi, F.; Mao, Y. Recent advances on metal oxide-based luminescence thermometry. *J. Mater. Chem. C* **2021**, *9*, 16410–16439. [CrossRef]
12. Martinez, L.P.; Mina Villarreal, M.C.; Zaza, C.; Barella, M.; Acuna, G.P.; Stefani, F.D.; Violi, I.L.; Gargiulo, J. Thermometries for Single Nanoparticles Heated with Light. *ACS Sens.* **2024**, *9*, 1049–1064. [CrossRef] [PubMed]
13. Chennappa, T.; Kamath, S.D. Review—Structural and Optical Interpretations on Phosphor-Based Optical Thermometry. *ECS J. Solid State Sci. Technol.* **2024**, *13*, 077002. [CrossRef]
14. Suo, H.; Zhao, X.; Zhang, Z.; Wang, Y.; Sun, J.; Jin, M.; Guo, C. Rational Design of Ratiometric Luminescence Thermometry Based on Thermally Coupled Levels for Bioapplications. *Laser Photon. Rev.* **2021**, *15*, 2000319. [CrossRef]
15. Rodríguez-Sevilla, P.; Marin, R.; Ximendes, E.; del Rosal, B.; Benayas, A.; Jaque, D. Luminescence Thermometry for Brain Activity Monitoring: A Perspective. *Front. Chem.* **2022**, *10*, 941861. [CrossRef]
16. van Swieten, T.P.; Meijerink, A.; Rabouw, F.T. Impact of Noise and Background on Measurement Uncertainties in Luminescence Thermometry. *ACS Photonics* **2022**, *9*, 1366–1374. [CrossRef] [PubMed]
17. Benedict, R. *Fundamentals of Temperature*, 3rd ed.; John Wiley & Sons. Inc.: New York, NY, USA, 1984.
18. Dramićanin, M. Temperature and Ways of Measuring It. In *Luminescence Thermometry*; Elsevier: Amsterdam, The Netherlands, 2018; pp. 13–32.
19. Kolesnikov, I.E.; Mamonova, D.V.; Kalinichev, A.A.; Kurochkin, M.A.; Medvedev, V.A.; Kolesnikov, E.Y.; Lähderanta, E.; Manshina, A.A. Construction of efficient dual activating ratiometric YVO_4:Nd^{3+}/Eu^{3+} nanothermometers using co-doped and mixed phosphors. *Nanoscale* **2020**, *12*, 5953–5960. [CrossRef] [PubMed]
20. Li, M.; You, F.; Liang, C.; He, Z. Ratiometric thermal sensing based on dual emission of YBO_3:Ce^{3+}, Tb^{3+}. *J. Alloys Compd.* **2020**, *833*, 155011. [CrossRef]
21. Avram, D.; Colbea, C.; Florea, M.; Tiseanu, C. Highly -sensitive near infrared luminescent nanothermometers based on binary mixture. *J. Alloys Compd.* **2019**, *785*, 250–259. [CrossRef]
22. Wang, L.; Lee, H.; Ju, D.Y. Impact of digital content on young children's reading interest and concentration for books. *Behav. Inf. Technol.* **2019**, *38*, 1–8. [CrossRef]
23. Matuszewska, C.; Elzbieciak-Piecka, K.; Marciniak, L. Transition Metal Ion-Based Nanocrystalline Luminescent Thermometry in $SrTiO_3$:Ni^{2+},Er^{3+} Nanocrystals Operating in the Second Optical Window of Biological Tissues. *J. Phys. Chem. C* **2019**, *123*, 18646–18653. [CrossRef]
24. Elzbieciak, K.; Bednarkiewicz, A.; Marciniak, L. Temperature sensitivity modulation through crystal field engineering in Ga^{3+} co-doped Gd_3Al_5-xGa_xO_{12}:Cr^{3+}, Nd^{3+} nanothermometers. *Sens. Actuators B Chem.* **2018**, *269*, 96–102. [CrossRef]
25. Chen, Y.; He, J.; Zhang, X.; Rong, M.; Xia, Z.; Wang, J.; Liu, Z.-Q. Dual-Mode Optical Thermometry Design in $Lu_3Al_5O_{12}$:Ce^{3+}/Mn^{4+} Phosphor. *Inorg. Chem.* **2020**, *59*, 1383–1392. [CrossRef]
26. Chen, D.; Liu, S.; Zhou, Y.; Wan, Z.; Huang, P.; Ji, Z. Dual-activator luminescence of RE/TM:$Y_3Al_5O_{12}$ (RE = Eu^{3+}, Tb^{3+}, Dy^{3+}; TM = Mn^{4+}, Cr^{3+}) phosphors for self-referencing optical thermometry. *J. Mater. Chem. C* **2016**, *4*, 9044–9051. [CrossRef]
27. Xie, X.; Ge, W.; Tian, Y.; Zhang, Q.; Yang, M.; Wu, C.; He, P.; Yin, H. $La_3Sc_2Ga_3O_{12}$:Cr^{3+}, Nd^{3+} near-infrared phosphor for nondestructive detection and luminescence thermometry. *Ceram. Int.* **2024**, *50*, 46098–46106. [CrossRef]
28. Zhu, B.; Wang, L.; Shi, Q.; Guo, H.; Qiao, J.; Cui, C.; Huang, P. Tb^{3+}/Mn^{4+} co-doped SrLaMgNbO6 green/red dual-emitting phosphors for optical thermometry. *Ceram. Int.* **2023**, *49*, 35285–35292. [CrossRef]
29. Lin, Y.; Zhao, L.; Jiang, B.; Mao, J.; Chi, F.; Wang, P.; Xie, C.; Wei, X.; Chen, Y.; Yin, M. Temperature-dependent luminescence of $BaLaMgNbO_6$:Mn^{4+}, Dy^{3+} phosphor for dual-mode optical thermometry. *Opt. Mater.* **2019**, *95*, 109199. [CrossRef]
30. Pan, Y.; Xie, X.; Huang, Q.; Gao, C.; Wang, Y.; Wang, L.; Yang, B.; Su, H.; Huang, L.; Huang, W. Inherently Eu^{2+}/Eu^{3+} Codoped Sc_2O_3 Nanoparticles as High-Performance Nanothermometers. *Adv. Mater.* **2018**, *30*, e1705256. [CrossRef]
31. Ćirić, A.; Stojadinović, S.; Ristić, Z.; Zeković, I.; Kuzman, S.; Antić, Ž.; Dramićanin, M.D. Supersensitive Sm^{2+}-Activated Al_2O_3 Thermometric Coatings for High-Resolution Multiple Temperature Read-Outs from Luminescence. *Adv. Mater. Technol.* **2021**, *6*, 2001201. [CrossRef]
32. Wang, S.; Westcott, S.; Chen, W. Nanoparticle Luminescence Thermometry. *J. Phys. Chem. B* **2002**, *106*, 11203–11209. [CrossRef]
33. Parobek, D.; Roman, B.J.; Dong, Y.; Jin, H.; Lee, E.; Sheldon, M.; Son, D.H. Exciton-to-Dopant Energy Transfer in Mn-Doped Cesium Lead Halide Perovskite Nanocrystals. *Nano Lett.* **2016**, *16*, 7376–7380. [CrossRef]
34. Nikolić, M.G.; Antić, Ž.; Ćulubrk, S.; Nedeljković, J.M.; Dramićanin, M.D. Temperature sensing with Eu^{3+} doped TiO_2 nanoparticles. *Sens. Actuators B Chem.* **2014**, *201*, 46–50. [CrossRef]
35. Dramićanin, M.D.; Antić, Ž.; Ćulubrk, S.; Ahrenkiel, S.P.; Nedeljković, J.M. Self-referenced luminescence thermometry with Sm^{3+} doped TiO_2 nanoparticles. *Nanotechnology* **2014**, *25*, 485501. [CrossRef] [PubMed]
36. Ćulubrk, S.; Lojpur, V.; Ahrenkiel, S.P.; Nedeljković, J.M.; Dramićanin, M.D. Non-contact thermometry with Dy^{3+} doped $Gd_2Ti_2O_7$ nano-powders. *J. Lumin.* **2016**, *170*, 395–400. [CrossRef]

37. Das, S.; Som, S.; Yang, C.-Y.; Chavhan, S.; Lu, C.-H. Structural evaluations and temperature dependent photoluminescence characterizations of Eu^{3+}-activated $SrZrO_3$ hollow spheres for luminescence thermometry applications. *Sci. Rep.* **2016**, *6*, 25787. [CrossRef] [PubMed]
38. Drabik, J.; Ledwa, K.; Marciniak, Ł. Implementing Defects for Ratiometric Luminescence Thermometry. *Nanomaterials* **2020**, *10*, 1333. [CrossRef]
39. Suta, M.; Meijerink, A. A Theoretical Framework for Ratiometric Single Ion Luminescent Thermometers—Thermodynamic and Kinetic Guidelines for Optimized Performance. *Adv. Theory Simul.* **2020**, *3*, 2000176. [CrossRef]
40. Suta, M.; Antić, Ž.; Đorđević, V.; Kuzman, S.; Dramićanin, M.D.; Meijerink, A. Making Nd^{3+} a Sensitive Luminescent Thermometer for Physiological Temperatures—An Account of Pitfalls in Boltzmann Thermometry. *Nanomaterials* **2020**, *10*, 543. [CrossRef]
41. Geitenbeek, R.G.; De Wijn, H.W.; Meijerink, A. Non-Boltzmann Luminescence in Na_yF_4:Eu^{3+}: Implications for Luminescence Thermometry. *Phys. Rev. Appl.* **2018**, *10*, 064006. [CrossRef]
42. Wade, S.A.; Collins, S.F.; Baxter, G.W. Fluorescence intensity ratio technique for optical fiber point temperature sensing. *J. Appl. Phys.* **2003**, *94*, 4743. [CrossRef]
43. Glais, E.; Đorđević, V.; Papan, J.; Viana, B.; Dramićanin, M.D. $MgTiO_3$:Mn^{4+} a multi-reading temperature nanoprobe. *RSC Adv.* **2018**, *8*, 18341–18346. [CrossRef] [PubMed]
44. Back, M.; Trave, E.; Ueda, J.; Tanabe, S. Ratiometric Optical Thermometer Based on Dual Near-Infrared Emission in Cr^{3+}-Doped Bismuth-Based Gallate Host. *Chem. Mater.* **2016**, *28*, 8347–8356. [CrossRef]
45. Ueda, J.; Back, M.; Brik, M.G.; Zhuang, Y.; Grinberg, M.; Tanabe, S. Ratiometric optical thermometry using deep red luminescence from $^4T_2$ and ^2E states of Cr^{3+} in $ZnGa_2O_4$ host. *Opt. Mater.* **2018**, *85*, 510–516. [CrossRef]
46. Back, M.; Ueda, J.; Xu, J.; Asami, K.; Brik, M.G.; Tanabe, S. Effective Ratiometric Luminescent Thermal Sensor by Cr^{3+}-Doped Mullite $Bi_2Al_4O_9$ with Robust and Reliable Performances. *Adv. Opt. Mater.* **2020**, *8*, 2000124. [CrossRef]
47. Dramićanin, M.D.; Marciniak, Ł.; Kuzman, S.; Piotrowski, W.; Ristić, Z.; Periša, J.; Evans, I.; Mitrić, J.; Đorđević, V.; Romčević, N.; et al. Mn^{5+}-activated $Ca_6Ba(PO_4)_4O$ near-infrared phosphor and its application in luminescence thermometry. *Light Sci. Appl.* **2022**, *11*, 279. [CrossRef]
48. Alrebdi, T.A.; Alodhayb, A.N.; Ristić, Z.; Dramićanin, M.D. Comparison of Performance between Single- and Multiparameter Luminescence Thermometry Methods Based on the Mn^{5+} Near-Infrared Emission. *Sensors* **2023**, *23*, 3839. [CrossRef] [PubMed]
49. Tian, X.; Wei, X.; Chen, Y.; Duan, C.; Yin, M. Temperature sensor based on ladder-level assisted thermal coupling and thermal-enhanced luminescence in $NaYF_4$:Nd^{3+}. *Opt. Express* **2014**, *22*, 30333. [CrossRef]
50. Li, L.; Qin, F.; Zhou, Y.; Zheng, Y.; Miao, J.; Zhang, Z. Three-energy-level-cascaded strategy for a more sensitive luminescence ratiometric thermometry. *Sens. Actuators A Phys.* **2020**, *304*, 111864. [CrossRef]
51. Periša, J.; Ćirić, A.; Zeković, I.; Đorđević, V.; Sekulić, M.; Antić, Ž.; Dramićanin, M.D. Exploiting High-Energy Emissions of $YAlO_3$:Dy^{3+} for Sensitivity Improvement of Ratiometric Luminescence Thermometry. *Sensors* **2022**, *22*, 7997. [CrossRef]
52. Ćirić, A.; Aleksić, J.; Barudžija, T.; Antić, Ž.; Đorđević, V.; Medić, M.; Periša, J.; Zeković, I.; Mitrić, M.; Dramićanin, M.D. Comparison of three ratiometric temperature readings from the Er^{3+} upconversion emission. *Nanomaterials* **2020**, *10*, 627. [CrossRef]
53. Yu, D.; Li, H.; Zhang, D.; Zhang, Q.; Meijerink, A.; Suta, M. One ion to catch them all: Targeted high-precision Boltzmann thermometry over a wide temperature range with Gd^{3+}. *Light Sci. Appl.* **2021**, *10*, 236. [CrossRef] [PubMed]
54. Ćirić, A.; Periša, J.; Zeković, I.; Antić, Ž.; Dramićanin, M.D. Multilevel-cascade intensity ratio temperature read-out of Dy^{3+} luminescence thermometers. *J. Lumin.* **2022**, *245*, 118795. [CrossRef]
55. Antić, Ž.; Ćirić, A.; Sekulić, M.; Periša, J.; Milićević, B.; Alodhayb, A.N.; Alrebdi, T.A.; Dramićanin, M.D. Thirty-Fold Increase in Relative Sensitivity of Dy^{3+} Luminescent Boltzmann Thermometers Using Multiparameter and Multilevel Cascade Temperature Readings. *Crystals* **2023**, *13*, 884. [CrossRef]
56. Souza, A.S.; Nunes, L.A.O.; Silva, I.G.N.; Oliveira, F.A.M.; da Luz, L.L.; Brito, H.F.; Felinto, M.C.F.C.; Ferreira, R.A.S.; Júnior, S.A.; Carlos, L.D.; et al. Highly-sensitive Eu^{3+} ratiometric thermometers based on excited state absorption with predictable calibration. *Nanoscale* **2016**, *8*, 5327–5333. [CrossRef]
57. Chang, N.C.; Gruber, J.B.; Leavitt, R.P.; Morrison, C.A. Optical spectra, energy levels, and crystal-field analysis of tripositive rare earth ions in Y_2O_3. I. Kramers ions in C_2 sites. *J. Chem. Phys.* **1982**, *76*, 3877–3889. [CrossRef]
58. Leavitt, R.P.; Gruber, J.B.; Chang, N.C.; Morrison, C.A. Optical spectra, energy levels, and crystal-field analysis of tripositive rare-earth ions in Y_2O_3. II. Non-Kramers ions in C_2 sites. *J. Chem. Phys.* **1982**, *76*, 4775–4788. [CrossRef]
59. Ćirić, A.; Zeković, I.; Medić, M.; Antić, Ž.; Dramićanin, M.D. Judd-Ofelt modelling of the dual-excited single band ratiometric luminescence thermometry. *J. Lumin.* **2020**, *225*, 117369. [CrossRef]
60. Zhou, S.; Li, X.; Wei, X.; Duan, C.; Yin, M. A new mechanism for temperature sensing based on the thermal population of $^7F_2$ state in Eu $^{3+}$. *Sens. Actuators B Chem.* **2016**, *231*, 641–645. [CrossRef]
61. Ćirić, A.; Marciniak, Ł.; Dramićanin, M.D. Luminescence intensity ratio squared—A new luminescence thermometry method for enhanced sensitivity. *J. Appl. Phys.* **2022**, *131*, 114501. [CrossRef]
62. Ćirić, A.; van Swieten, T.; Periša, J.; Meijerink, A.; Dramićanin, M.D. Twofold increase in the sensitivity of Er^{3+}/Yb^{3+} Boltzmann thermometer. *J. Appl. Phys.* **2023**, *133*, 194501. [CrossRef]
63. Qiu, X.; Zhou, Q.; Zhu, X.; Wu, Z.; Feng, W.; Li, F. Ratiometric upconversion nanothermometry with dual emission at the same wavelength decoded via a time-resolved technique. *Nat. Commun.* **2020**, *11*, 4. [CrossRef] [PubMed]

64. Mykhaylyk, V.; Kraus, H.; Zhydachevskyy, Y.; Tsiumra, V.; Luchechko, A.; Wagner, A.; Suchocki, A. Multimodal Non-Contact Luminescence Thermometry with Cr-Doped Oxides. *Sensors* **2020**, *20*, 5259. [CrossRef] [PubMed]
65. Li, H.; Heydari, E.; Li, Y.; Xu, H.; Xu, S.; Chen, L.; Bai, G. Multi-Mode Lanthanide-Doped Ratiometric Luminescent Nanothermometer for Near-Infrared Imaging within Biological Windows. *Nanomaterials* **2023**, *13*, 219. [CrossRef] [PubMed]
66. Savchuk, O.; Carvajal Marti, J.J.; Cascales, C.; Haro-Gonzalez, P.; Sanz-Rodríguez, F.; Aguilo, M.; Diaz, F. Bifunctional Tm^{3+},Yb^{3+}:$GdVO_4$@SiO_2 Core-Shell Nanoparticles in HeLa Cells: Upconversion Luminescence Nanothermometry in the First Biological Window and Biolabelling in the Visible. *Nanomaterials* **2020**, *10*, 993. [CrossRef]
67. Wang, J.; Lu, J.; Wu, Y.; Song, M. Luminescence of Mn^{4+} in a Zero-Dimensional Organic–Inorganic Hybrid Phosphor $[N(CH_3)_4]_2ZrF_6$ for Dual-Mode Temperature Sensing. *Materials* **2022**, *15*, 6543. [CrossRef]
68. Chen, J.Y.; Chen, J.Q.; Li, L.J.; Zhang, W.N.; Chen, L.P.; Guo, H. A four-mode high-sensitive optical thermometer based on $Ca_3LiZnV_3O_{12}$:Sm_{3+} phosphors. *Mater. Today Chem.* **2023**, *29*, 101409. [CrossRef]
69. Shen, Y.; Santos, H.D.A.; Ximendes, E.C.; Lifante, J.; Sanz-Portilla, A.; Monge, L.; Fernández, N.; Chaves-Coira, I.; Jacinto, C.; Brites, C.D.S.; et al. Ag_2S Nanoheaters with Multiparameter Sensing for Reliable Thermal Feedback during In Vivo Tumor Therapy. *Adv. Funct. Mater.* **2020**, *30*, 2002730. [CrossRef]
70. Maturi, F.E.; Brites, C.D.S.; Ximendes, E.C.; Mills, C.; Olsen, B.; Jaque, D.; Ribeiro, S.J.L.; Carlos, L.D. Going Above and Beyond: A Tenfold Gain in the Performance of Luminescence Thermometers Joining Multiparametric Sensing and Multiple Regression. *Laser Photon. Rev.* **2021**, *15*, 2100301. [CrossRef]
71. Aseev, V.A.; Borisevich, D.A.; Khodasevich, M.A.; Kuz'menko, N.K.; Fedorov, Y.K. Calibration of Temperature by Normalized Up-Conversion Fluorescence Spectra of Germanate Glasses and Glass Ceramics Doped with Erbium and Ytterbium Ions. *Opt. Spectrosc.* **2021**, *129*, 297–302. [CrossRef]
72. Borisov, E.V.; Kalinichev, A.A.; Kolesnikov, I.E. ZnTe Crystal Multimode Cryogenic Thermometry Using Raman and Luminescence Spectroscopy. *Materials* **2023**, *16*, 1311. [CrossRef]
73. Lewis, C.; Erikson, J.W.; Sanchez, D.A.; McClure, C.E.; Nordin, G.P.; Munro, T.R.; Colton, J.S. Use of Machine Learning with Temporal Photoluminescence Signals from CdTe Quantum Dots for Temperature Measurement in Microfluidic Devices. *ACS Appl. Nano Mater.* **2020**, *3*, 4045–4053. [CrossRef] [PubMed]
74. Ximendes, E.; Marin, R.; Carlos, L.D.; Jaque, D. Less is more: Dimensionality reduction as a general strategy for more precise luminescence thermometry. *Light Sci. Appl.* **2022**, *11*, 237. [CrossRef]
75. Šević, D.; Vlašić, A.; Rabasović, M.; Savić-Šević, S.; Rabasović, M.; Nikolić, M.; Murić, B.; Marinković, B.; Križan, J. Temperature effects on luminescent properties of Sr_2CeO_4:Eu^{3+} nanophosphor: A machine learning approach. *Tehnika* **2020**, *75*, 279–283. [CrossRef]
76. Rajčić, A.; Ristić, Z.; Periša, J.; Milićević, B.; Aldawood, S.; Alodhayb, A.N.; Antić, Ž.; Dramićanin, M.D. Using Principal Component Analysis for Temperature Readings from YF_3:Pr_{3+} Luminescence. *Technologies* **2024**, *12*, 131. [CrossRef]
77. Liu, L.; Zhong, K.; Munro, T.; Alvarado, S.; Côte, R.; Creten, S.; Fron, E.; Ban, H.; Van der Auweraer, M.; Roozen, N.B.; et al. Wideband fluorescence-based thermometry by neural network recognition: Photothermal application with 10 ns time resolution. *J. Appl. Phys.* **2015**, *118*, 184906. [CrossRef]
78. Cui, J.; Xu, W.; Yao, M.; Zheng, L.; Hu, C.; Zhang, Z.; Sun, Z. Convolutional neural networks open up horizons for luminescence thermometry. *J. Lumin.* **2023**, *256*, 119637. [CrossRef]
79. Xu, W.; Xu, C.; Cui, J.; Hu, C.; Wen, G.; Zheng, L.; Zhang, Z.; Sun, Z.; Zhang, Y. Luminescence thermometry driven by a support vector machine: A strategy toward precise thermal sensing. *Opt. Lett.* **2024**, *49*, 606. [CrossRef]
80. Jelic, J.Z.; Dencevski, A.; Rabasovic, M.D.; Krizan, J.; Savic-Sevic, S.; Nikolic, M.G.; Aguirre, M.H.; Sevic, D.; Rabasovic, M.S. Improving the Two-Color Temperature Sensing Using Machine Learning Approach: $GdVO_4$:Sm^{3+} Prepared by Solution Combustion Synthesis (SCS). *Photonics* **2024**, *11*, 642. [CrossRef]
81. LeCun, Y.; Bengio, Y.; Hinton, G. Deep learning. *Nature* **2015**, *521*, 436–444. [CrossRef]
82. Liu, L.; Creten, S.; Firdaus, Y.; Agustin Flores Cuautle, J.J.; Kouyaté, M.; Van der Auweraer, M.; Glorieux, C. Fluorescence spectra shape based dynamic thermometry. *Appl. Phys. Lett.* **2014**, *104*, 031902. [CrossRef]
83. Munro, T.; Liu, L.; Glorieux, C.; Ban, H. CdSe/ZnS quantum dot fluorescence spectra shape-based thermometry via neural network reconstruction. *J. Appl. Phys.* **2016**, *119*, 214903. [CrossRef]
84. Li, Z.; Liu, F.; Yang, W.; Peng, S.; Zhou, J. A Survey of Convolutional Neural Networks: Analysis, Applications, and Prospects. *IEEE Trans. Neural Netw. Learn. Syst.* **2022**, *33*, 6999–7019. [CrossRef] [PubMed]
85. Hochreiter, S.; Schmidhuber, J. Long Short-Term Memory. *Neural Comput.* **1997**, *9*, 1735–1780. [CrossRef] [PubMed]
86. Cai, T.; Deng, Z.; Park, Y.; Mohammadshahi, S.; Liu, Y.; Kim, K.C. Acquisition of kHz-frequency two-dimensional surface temperature field using phosphor thermometry and proper orthogonal decomposition assisted long short-term memory neural networks. *Int. J. Heat Mass Transf.* **2021**, *165*, 120662. [CrossRef]
87. Ćirić, A.; Ristić, Z.; Gavrilović, T.; Periša, J.; Medić, M.; Dramićanin, M.D. Sensor fusion luminescence thermometry better together. *arXiv* **2024**, arXiv:2409.03479.